Supporting Materials

Mechanistic Insights into the Two-Phase Synthesis of Heteroleptic Au Nanoclusters

Xiangyu Wang,[†a] Shanshan Wang,[†a] Shuyu Qian,[a] Naiwei Liu,[a]

Xinyue Dou,[a] and Xun Yuan*[a,b]

[a] *College of Materials Science and Engineering, Qingdao University of Science and Technology, Qingdao 266042, P. R. China.*

[b] *Institute of Bioengineering and Nanotechnology, 31 Biopolis Way, The Nanos, Singapore 138669, Singapore.*

[†] *These two authors contributed equally to this paper.*

[*] *Corresponding author. Tel.: +8684023177. E-mail address: yuanxun@qust.edu.cn.*

Experimental section:

Materials and Instrumentation.

Ultrapure Millipore water (18.2 MΩ) was used in all the experiments. All glassware and PTFE magnetic stirring bars were washed with aqua regia (HCl/HNO_3 volume ratio = 3:1), rinsed with copious ethanol and water, and dried in an oven before use. 1-Adamantanethiol (Adm), benzeneselenol (PhSe), hydrogen tetrachloroaurate (III) hydrate ($HAuCl_4 \cdot 3H_2O$), cyclohexanethiol (Cyc), and 4-methylbenzenethiol (MBT) from Sigma-Aldrich; Sodium borohydride ($NaBH_4$) from Merck; Toluene, and ethanol from Fisher; N,N-dimethylformamide (DMF) from J. T. Baker; and sodium hydroxide (NaOH) from Kanto Chemical were used as received.

UV–Vis spectra were recorded on an Agilent 8453 UV–visible spectrometer system. Transmission electron microscope (TEM) images of samples were acquired on a JEOL JEM 2100F microscope. Fourier transform infrared (FTIR) spectra were recorded on a Bruker Vertex 70 FTIR spectrometer. The molecular formulas of Au NCs and Au(I) complexes were determined by electrospray ionization mass spectrometry (ESI-MS) on an Agilent 6210 Time-of-Flight LC/MS system. Samples of 5 μL were directly injected into the chamber. Typical instrument parameters: flow rate of the elution (acetonitrile), 0.3 mL·min-1; capillary voltage, 3.5 – 4 kV; nebulizer, 48 psig; dry gas, 6 – 7 L·min-1 at 250 – 350 oC; m/z range, 100 – 10000. The binding energies of ligand-Au(I) complexes were calculated by utilizing the Gaussian 09 program package. The geometry optimizations were performed at the density functional theory (DFT) level, and the Becke's three parameter hybrid functional with the Lee-Yang-Parr correlation functional (B3LYP) method was employed to do the calculations. The 6-31G basic from the Gaussian basis set library has been used in all the calculations. The binding energies were obtained at the B3LYP level in conjunction with the 6-311+G (2d, p) basis set with the use of the above optimized geometries, i.e., B3LYP/6-311+G (2d, p) //B3LYP/6-31G.

Synthesis of Adm_PhSe-Protected Au NCs.

Synthesis of $Au_{41}(Adm)_{26-x}(PhSe)_x$ NCs.

Aqueous solution of $HAuCl_4$ (50 mM) was prepared with ultrapure water while hydrophobic ligands (50 mM) were dissolved in toluene. Aqueous solution of $NaBH_4$ was prepared by dissolving 43 mg of $NaBH_4$ powder in 10 mL of 0.2 M NaOH solution. In a typical synthesis of $Au_{41}(Adm)_{26-x}(PhSe)_x$ NCs, toluene solutions of Adm ligand (50 mM, 150 μL) and PhSe ligand (50 mM, 100 μL), and an aqueous solution of $HAuCl_4$ (50 mM, 100 μL) were separately added in DMF (5 mL) under stirring condition to form ligand-Au(I) complexes. An aqueous NaOH solution (1 M, 0.4 mL) and 4.8 mL of toluene were then introduced into the reaction mixture, followed by the addition of 0.1 mL of $NaBH_4$ solution. The $Au_{41}(Adm)_{26-x}(PhSe)_x$ NCs were collected after stirring of 3 h for further characterizations.

Here it should be mentioned that the Adm-to-PhSe ratios can be adjusted to 37.5 μL : 175 μL (1:7), 75 μL : 150 μL (2 : 6), 112.5 μL : 125 μL (3 : 5), 150 μL : 100 μL (4 : 4), 187.5 μL : 75 μL (5 : 3), 225 μL : 50 μL (6 : 2), and 25 μL : 262.5 μL (7 : 1), and a series of $Au_{41}(Adm)_{26-x}(PhSe)_x$ NC samples can be synthesized under the same synthetic conditions.

In addition, by using Adm (50 mM, 300 μL) as protecting ligand, homoleptic $Au_{23}(Adm)_{16}$ NCs can be synthesized under the same synthetic conditions; By using PhSe (50 mM, 200 μL) as protecting ligand, homoleptic $Au_{61}(PhSe)_{31}$ NCs can be synthesized under the same synthetic conditions.

Synthesis of $Au_{23}(Adm)_{16-x}(PhSe)_x$ NCs.

In a typical synthesis of $Au_{23}(Adm)_{16-x}(PhSe)_x$ NCs, toluene solutions of Adm ligand (50 mM, 150 μL) and PhSe ligand (50 mM, 100 μL), and an aqueous solution of $HAuCl_4$ (50 mM, 100 μL) were separately added in water (0.5 mL) under stirring condition, followed by adding certain volume of DMF (4.5 mL) as the miscible solvent to facilitate the formation of ligand-Au(I) complexes. An aqueous NaOH solution (1 M, 0.4 mL) and 4.8 mL of toluene were then

introduced into the reaction mixture, followed by the addition of 0.1 mL of $NaBH_4$ solution. The $Au_{23}(Adm)_{16-x}(PhSe)_x$ NCs were collected after stirring of 3 h for further characterizations.

Here it should be mentioned that the Adm-to-PhSe ratios can be adjusted to 37.5 μL : 175 μL (1:7), 75 μL : 150 μL (2 : 6), 112.5 μL : 125 μL (3 : 5), 150 μL : 100 μL (4 : 4), 187.5 μL : 75 μL (5 : 3), 225 μL : 50 μL (6 : 2), and 25 μL : 262.5 μL (7 : 1), and a series of $Au_{23}(Adm)_{16-x}(PhSe)_x$ NC samples can be synthesized under the same synthetic conditions.

In addition, by using Adm (50 mM, 300 μL) as protecting ligand, homoleptic $Au_{15}(Adm)_{12}$ NCs can be synthesized under the same synthetic conditions; By using PhSe (50 mM, 200 μL) as protecting ligand, homoleptic $Au_{40}(PhSe)_{24}$ NCs can be synthesized under the same synthetic conditions.

Synthesis of Adm_Cyc-Protected Au_{15} NCs

In a typical synthesis of $Au_{15}(Adm)_{12-x}(Cyc)_x$ NCs, toluene solutions of Adm ligand (50 mM, 150 μL) and Cyc ligand (50 mM, 100 μL), and an aqueous solution of $HAuCl_4$ (50 mM, 100 μL) were separately added in water (0.5 mL) under stirring condition, followed by adding certain volume of DMF (4.5 mL) as the miscible solvent to facilitate the formation of ligand-Au(I) complexes. An aqueous NaOH solution (1 M, 0.4 mL) and 4.8 mL of toluene were then introduced into the reaction mixture, followed by the addition of 0.1 mL of $NaBH_4$ solution. The $Au_{15}(Adm)_{12-x}(Cyc)_x$ NCs were collected after stirring of 3 h for further characterizations.

Here it should be mentioned that the Adm-to-Cyc ratios can be adjusted to 25 μL : 175 μL (1 : 7), 50 μL : 150 μL (2 : 6), 75 μL : 125 μL (3 : 5), 100 μL : 100 μL (4 : 4), 125 μL : 75 μL (5 : 3), 150 μL : 50 μL (6 : 2), and 175 μL : 25 μL (7 : 1), and a series of $Au_{15}(Adm)_{12-x}(Cyc)_x$ NCs NC samples can be synthesized under the same synthetic conditions.

In addition, by using Adm (50 mM, 200 μL) as protecting ligand, homoleptic $Au_{15}(Adm)_{12}$ NCs can be synthesized under the same synthetic conditions; By using Cyc (50 mM, 200 μL) as protecting ligand, homoleptic $Au_{23}(Cyc)_{16}$ NCs can be synthesized under the same synthetic conditions.

Synthesis of Bi-Ligand Cyc_MBT-Protected Au_{23} NCs

In a typical synthesis of $Au_{23}(Cyc)_{16-x}(MBT)_x$ NCs, toluene solutions of Cyc ligand (50 mM, 100 μL) and MBT ligand (50 mM, 100 μL), and an aqueous solution of $HAuCl_4$ (50 mM, 100 μL) were separately added in water (0.5 mL) under stirring condition, followed by adding certain volume of DMF (4.5 mL) as the miscible solvent to facilitate the formation of ligand-Au(I) complexes. An aqueous NaOH solution (1 M, 0.4 mL) and 4.8 mL of toluene were then introduced into the reaction mixture, followed by the addition of 0.1 mL of $NaBH_4$ solution. The $Au_{23}(Cyc)_{16-x}(MBT)_x$ NCs were collected after stirring of 3 h for further characterizations.

Here it should be mentioned that the Cyc-to-MBT ratios can be adjusted to 25 μL : 175 μL (1 : 7), 50 μL : 150 μL (2 : 6), 75 μL : 125 μL (3 : 5), 100 μL : 100 μL (4 : 4), 125 μL : 75 μL (5 : 3), 150 μL : 50 μL (6 : 2), and 175 μL : 25 μL (7 : 1), and a series of $Au_{23}(Cyc)_{16-x}(MBT)_x$ NC samples can be synthesized under the same synthetic conditions.

In addition, by using Cyc (50 mM, 200 μL) as protecting ligand, homoleptic $Au_{23}(Cyc)_{16}$ NCs can be synthesized under the same synthetic conditions; By using MBT (50 mM, 200 μL) as protecting ligand, homoleptic $Au_{25}(MBT)_{18}$ NCs can be synthesized under the same synthetic conditions.

Supplementary figures:

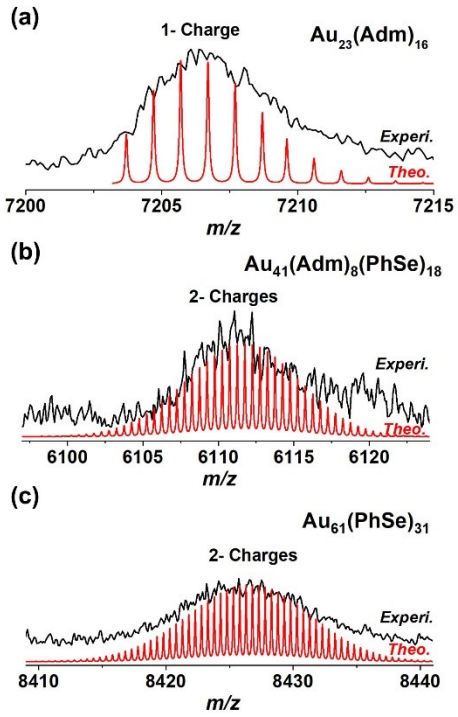

Figure S1. Isotope patterns acquired theoretically (red curve) and experimentally (black curve) for (a) homoleptic $Au_{23}(Adm)_{16}$ NCs, (b) heteroleptic $Au_{41}(Adm)_8(PhSe)_{18}$ NCs, and (c) homoleptic $Au_{61}(PhSe)_{31}$ NCs.

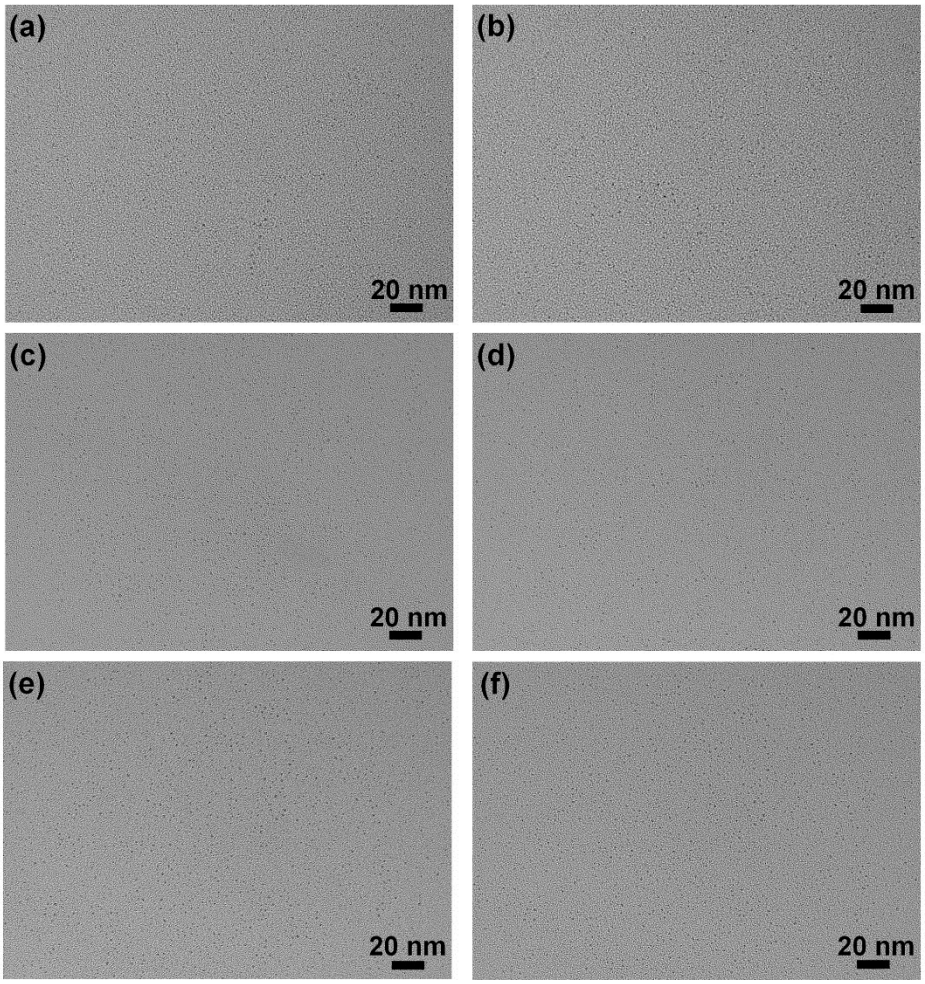

Figure S2. The representative TEM images of the (a) $Au_{23}(Adm)_{16}$ NCs, (b) $Au_{41}(Adm)_8(PhSe)_{18}$ NCs, (c) $Au_{61}(PhSe)_{31}$ NCs, (d) $Au_{15}(Adm)_{12}$ NCs, (e) $Au_{15}(Adm)_{6\text{-}10}(Cyc)_{6\text{-}2}$ NCs, and (f) $Au_{23}(Cyc)_{16}$ NCs.

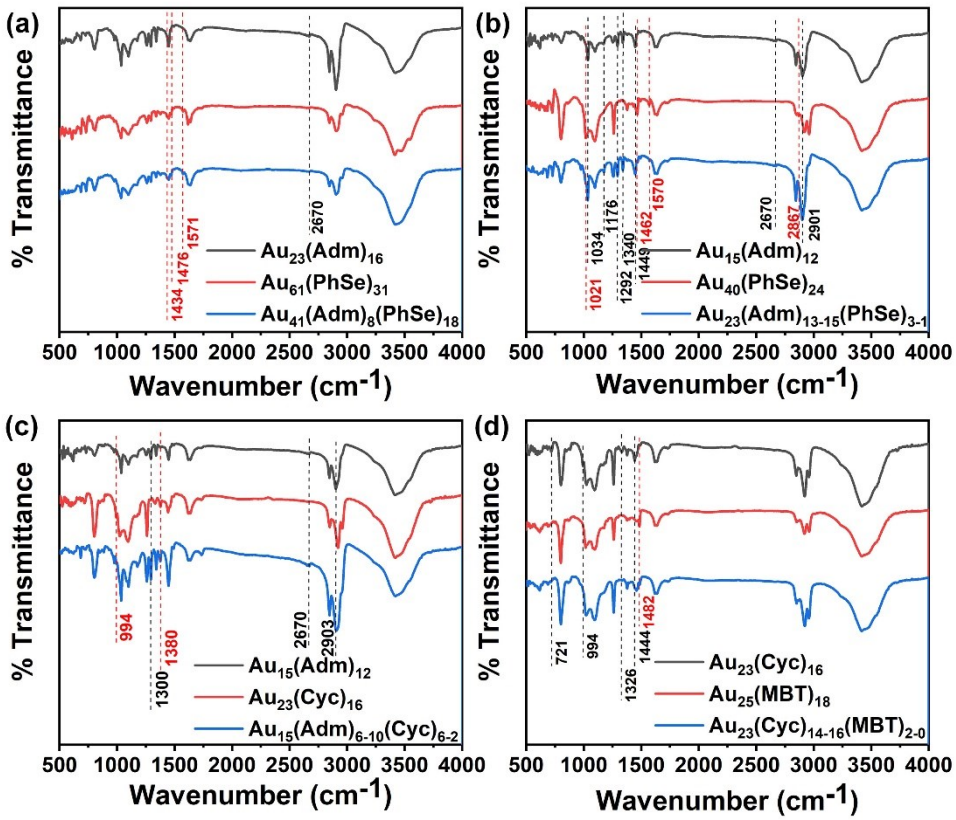

Figure S3. (a) FTIR spectra of the $Au_{23}(Adm)_{16}$ NCs, $Au_{61}(PhSe)_{31}$ NCs, and $Au_{41}(Adm)_8(PhSe)_{18}$ NCs. (b) FTIR spectra of the $Au_{15}(Adm)_{12}$ NCs, $Au_{40}(PhSe)_{24}$ NCs, and $Au_{23}(Adm)_{13\text{-}15}(PhSe)_{3\text{-}1}$ NCs. (c) FTIR spectra of the $Au_{15}(Adm)_{12}$ NCs, $Au_{23}(Cyc)_{16}$ NCs, and $Au_{15}(Adm)_{6\text{-}10}(Cyc)_{6\text{-}2}$ NCs. (d) FTIR spectra of the $Au_{23}(Cyc)_{16}$ NCs, $Au_{25}(MBT)_{16}$ NCs, and $Au_{23}(Cyc)_{14\text{-}16}(MBT)_{2\text{-}0}$ NCs.

Note I: As shown in Figure S3, we compared the FTIR spectra of homoleptic Au NCs with that of heteroleptic ones. Of note, the characteristic peaks of the FTIR spectra (solid black curves) of homoleptic $Au_{23}(Adm)_{16}$ NCs (Figure S3a), $Au_{15}(Adm)_{12}$ NCs (Figure S3b), $Au_{15}(Adm)_{12}$ NCs (Figure S3c), and $Au_{23}(Cyc)_{16}$ NCs (Figure S3d) were labelled with black dashed lines, which are separately different from that of (solid red curves) of the homoleptic $Au_{61}(PhSe)_{31}$ NCs (Figure S3a), $Au_{40}(PhSe)_{24}$ NCs (Figure S3b), $Au_{23}(Cyc)_{16}$ NCs (Figure S3c), and $Au_{25}(MBT)_{16}$ NCs (Figure S3d) labelled with red dashed lines. However, all these features can be inherited by their heteroleptic analogues, i.e., $Au_{41}(Adm)_8(PhSe)_{18}$ NCs (Figure S3a), $Au_{23}(Adm)_{13\text{-}15}(PhSe)_{3\text{-}1}$ NCs (Figure S3b), $Au_{15}(Adm)_{6\text{-}10}(Cyc)_{6\text{-}2}$ NCs (Figure S3c), and $Au_{23}(Cyc)_{14\text{-}16}(MBT)_{2\text{-}0}$ NCs (Figure S3d). These FTIR results suggest the successful synthesis of heteroleptic Au NCs.

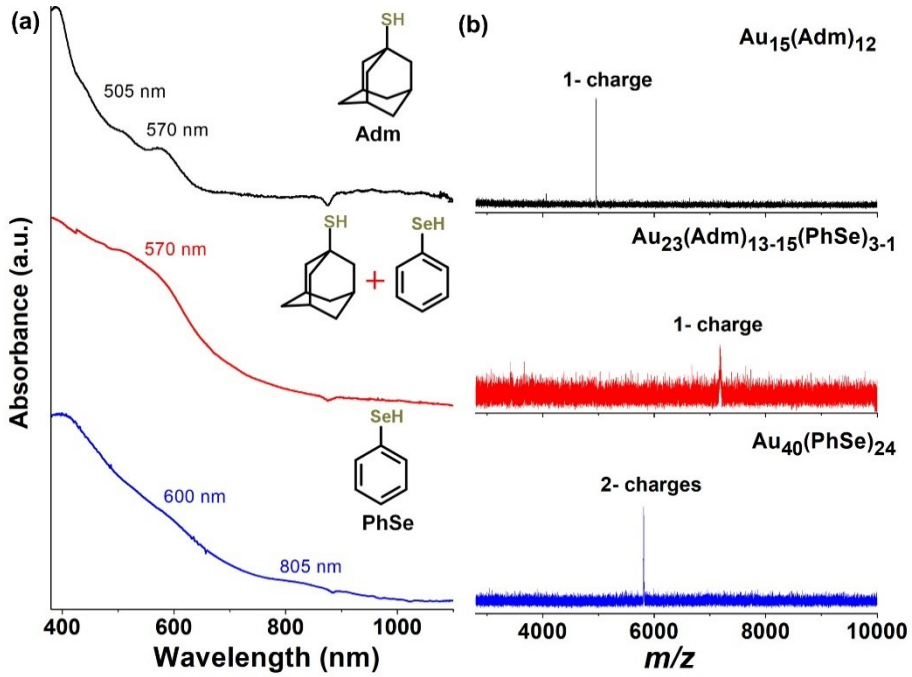

Figure S4. Eclectic effect of binary ligands on the size control of Au NCs. (a) UV−vis absorption and (b) ESI-MS spectra of homoleptic $Au_{15}(Adm)_{12}$ NCs (black curve), heteroleptic $Au_{23}(Adm)_{13–15}(PhSe)_{3–1}$ NCs (red curve), and homoleptic $Au_{40}(PhSe)_{24}$ NCs (blue curve).

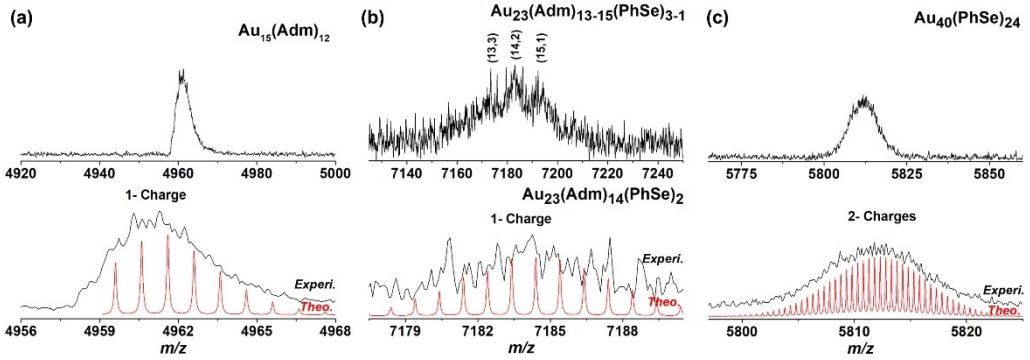

Figure S5. Enlarged ESI-MS spectra (upper panel) and isotope patterns (lower panel) acquired theoretically (red curve) and experimentally (black curve) for (a) homoleptic $Au_{15}(Adm)_{12}$ NCs, (b) heteroleptic $Au_{23}(Adm)_{13–15}(PhSe)_{3–1}$ NCs, and (c) homoleptic $Au_{40}(PhSe)_{24}$ NCs. The numbers (13,3), (14,2), and (15,1) labelled in the upper panel of Figure S5b represent $Au_{23}(Adm)_{13}(PhSe)_3$ NCs, $Au_{23}(Adm)_{14}(PhSe)_2$ NCs, and $Au_{23}(Adm)_{15}(PhSe)_1$ NCs, respectively.

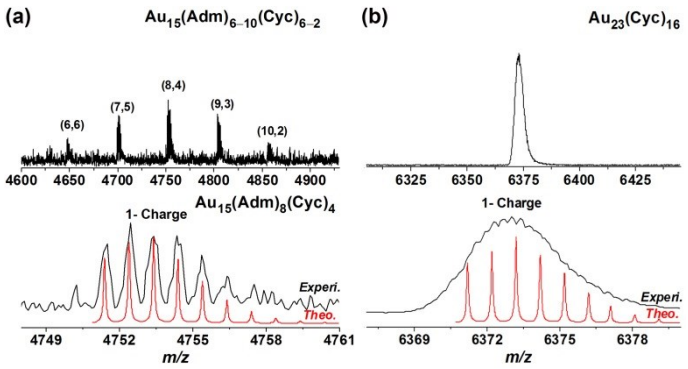

Figure S6. Enlarged ESI-MS spectra (upper panel) and isotope patterns (lower panel) acquired theoretically (red curve) and experimentally (black curve) for (a) heteroleptic $Au_{15}(Adm)_{6–10}(Cyc)_{6–2}$ NCs, and (b) homoleptic $Au_{23}(Cyc)_{16}$ NCs. The ESI-MS analysis for homoleptic $Au_{15}(Adm)_{12}$ NCs is shown in Figure S5a. The numbers (6,6), (7,5), (8,4), (9,3), and (10,2) labelled in the upper panel of Figure S6a represent $Au_{15}(Adm)_6(Cyc)_6$ NCs, $Au_{15}(Adm)_7(Cyc)_5$ NCs, $Au_{15}(Adm)_8(Cyc)_4$ NCs, $Au_{15}(Adm)_9(Cyc)_3$ NCs, and $Au_{15}(Adm)_{10}(Cyc)_2$ NCs, respectively.

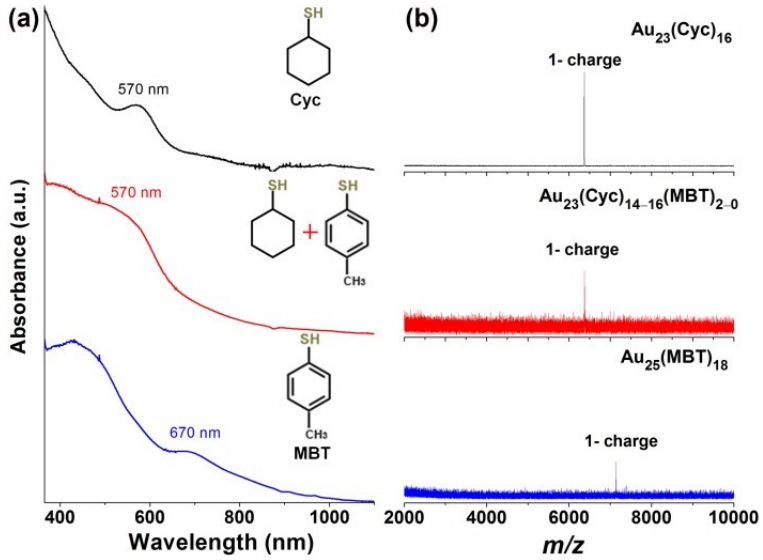

Figure S7. Competitive effect of binary ligands on the size control of Au NCs. (a) UV−vis absorption and (b) ESI-MS spectra of homoleptic $Au_{23}(Cyc)_{16}$ NCs (black curve), heteroleptic $Au_{23}(Cyc)_{14–16}(MBT)_{2–0}$ NCs (red curve), and homoleptic $Au_{25}(MBT)_{18}$ NCs (blue curve).

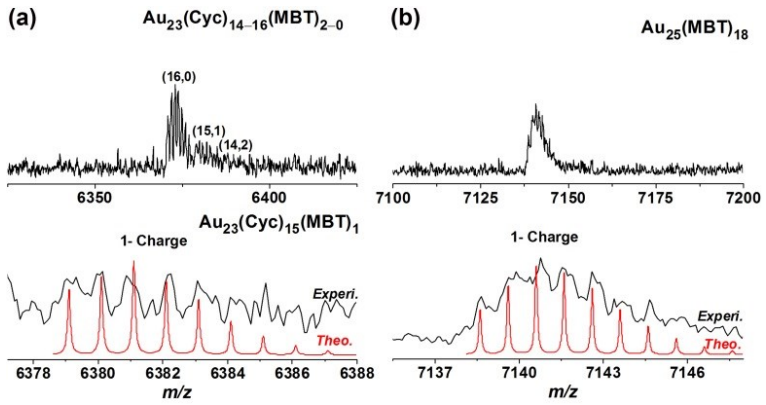

Figure S8. Enlarged ESI-MS spectra (upper panel) and isotope patterns (lower panel) acquired theoretically (red curve) and experimentally (black curve) for (a) heteroleptic $Au_{23}(Cyc)_{14-16}(MBT)_{2-0}$ NCs, and (b) homoleptic $Au_{25}(MBT)_{18}$ NCs. The ESI-MS analysis for homoleptic $Au_{23}(Cyc)_{16}$ NCs is shown in Figure S6b. The numbers (16,0), (15,1), and (14,2) labelled in the upper panel of Figure S8a represent $Au_{23}(Cyc)_{16}(MBT)_0$ NCs, $Au_{23}(Cyc)_{15}(MBT)_1$ NCs, and $Au_{23}(Cyc)_{14}(MBT)_2$ NCs, respectively.

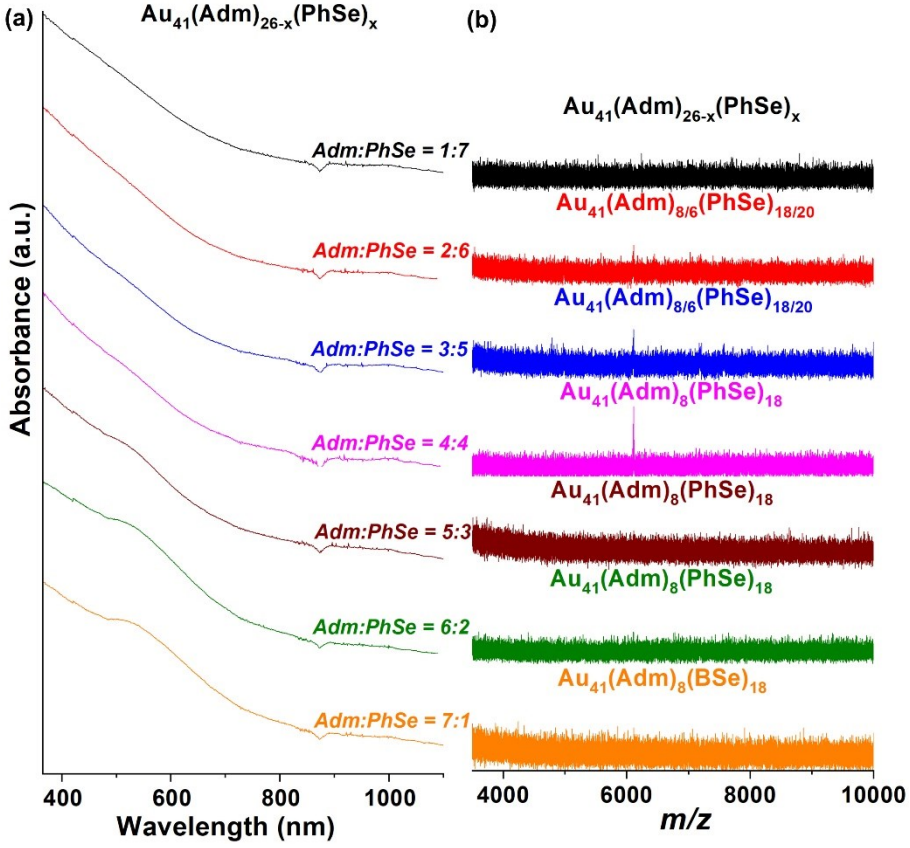

Figure S9. (a) UV−vis absorption and (b) ESI-MS spectra of heteroleptic $Au_{41}(Adm)_{26-x}(PhSe)_x$ NCs synthesized with the feeding ratios of Adm : PhSe = 1 : 7 (black curve), 2 : 6 (red curve), 3 : 5 (blue curve), 4 : 4 (pink curve), 5 : 3 (wine curve), 6 : 2 (green curve), and 7 : 1 (orange curve).

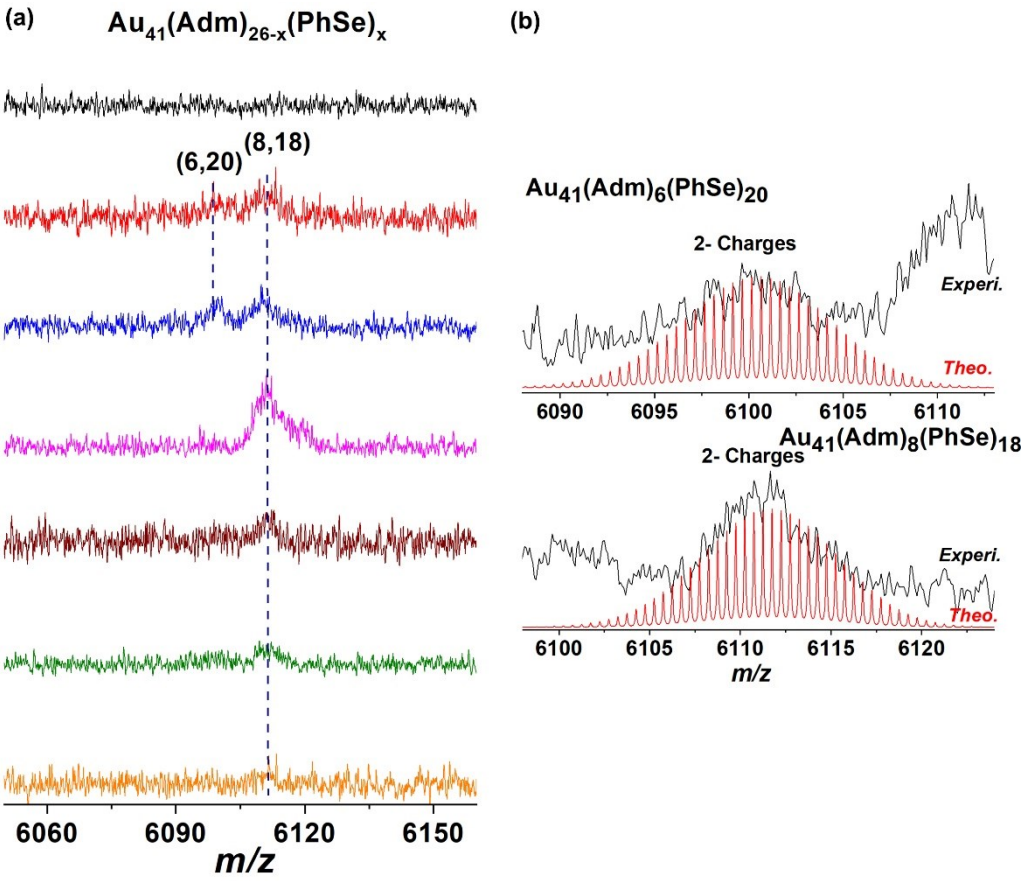

Figure S10. (a) Enlarged ESI-MS spectra of heteroleptic $Au_{41}(Adm)_{26-x}(PhSe)_x$ NCs synthesized with the feeding ratios of Adm : PhSe = 1:7 (black curve), 2 : 6 (red curve), 3 : 5 (blue curve), 4 : 4 (pink curve), 5 : 3 (wine curve), 6 : 2 (green curve), and 7 : 1 (orange curve). (b) Isotope patterns acquired theoretically (red curve) and experimentally (black curve) for $Au_{41}(Adm)_6(PhSe)_{20}$ NC species (upper panel) and $Au_{41}(Adm)_8(PhSe)_{18}$ NC species (lower panel).

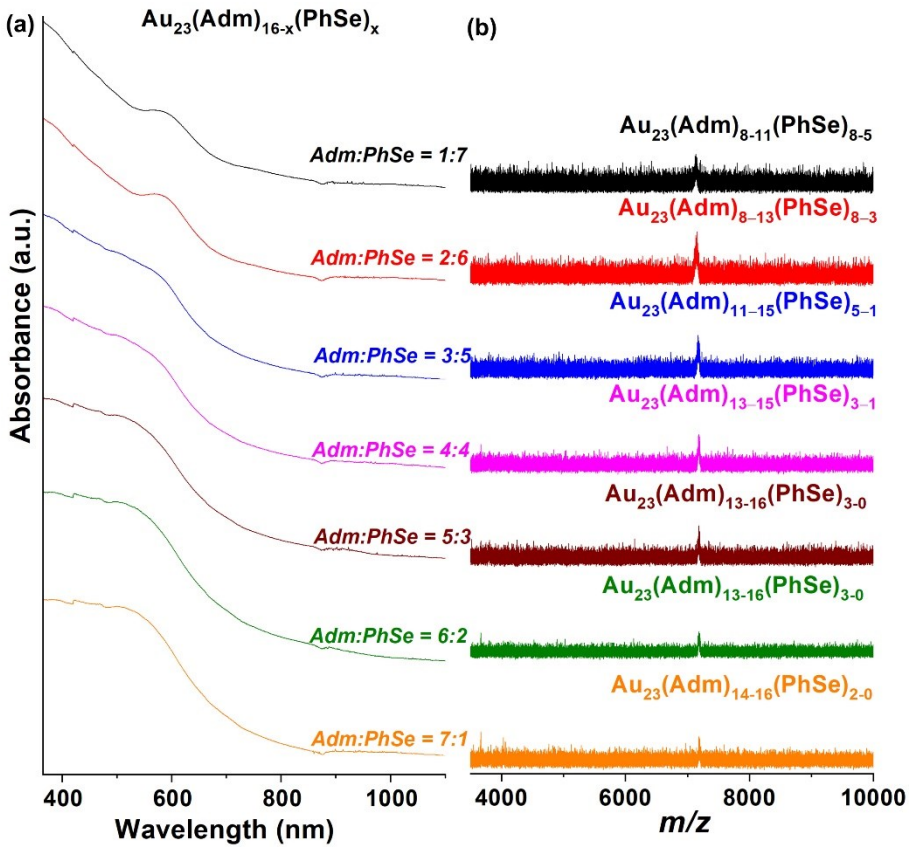

Figure S11. (a) UV−vis absorption and (b) ESI-MS spectra of heteroleptic $Au_{23}(Adm)_{16-x}(PhSe)_x$ NCs synthesized with the feeding ratios of Adm : PhSe = 1 : 7 (black curve), 2 : 6 (red curve), 3 : 5 (blue curve), 4 : 4 (pink curve), 5 : 3 (wine curve), 6 : 2 (green curve), and 7 : 1 (orange curve).

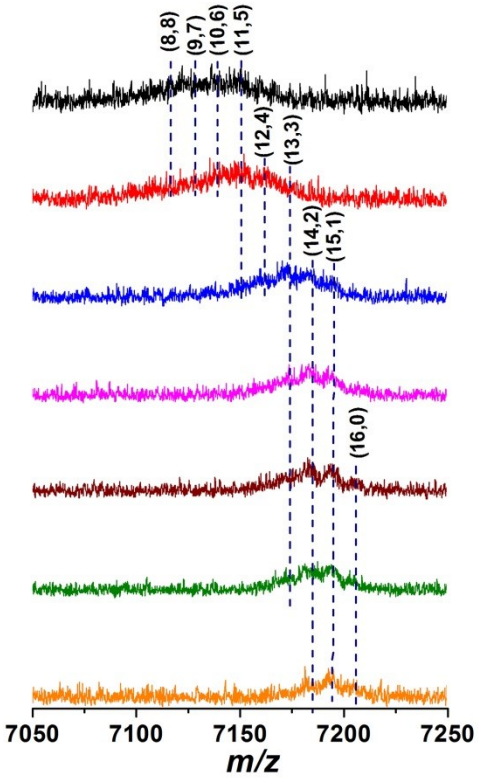

Figure S12. Enlarged ESI-MS spectra of heteroleptic $Au_{23}(Adm)_{16-x}(PhSe)_x$ NCs synthesized with the feeding ratios of Adm : PhSe = 1 : 7 (black curve), 2 : 6 (red curve), 3 : 5 (blue curve), 4 : 4 (pink curve), 5 : 3 (wine curve), 6 : 2 (green curve), and 7 : 1 (orange curve). The numbers (8, 8), (9, 7), (10, 6), (11, 5), (12, 4), (13, 3), (14, 2), (15, 1), and (16, 0) labelled in the Figure represent $Au_{23}(Adm)_8(PhSe)_8$ NCs, $Au_{23}(Adm)_9(PhSe)_7$ NCs, $Au_{23}(Adm)_{10}(PhSe)_6$ NCs, $Au_{23}(Adm)_{11}(PhSe)_5$ NCs, $Au_{23}(Adm)_{12}(PhSe)_4$ NCs, $Au_{23}(Adm)_{13}(PhSe)_3$ NCs, $Au_{23}(Adm)_{14}(PhSe)_2$ NCs, $Au_{23}(Adm)_{15}(PhSe)_1$ NCs, and $Au_{23}(Adm)_{16}(PhSe)_0$ NCs, respectively.

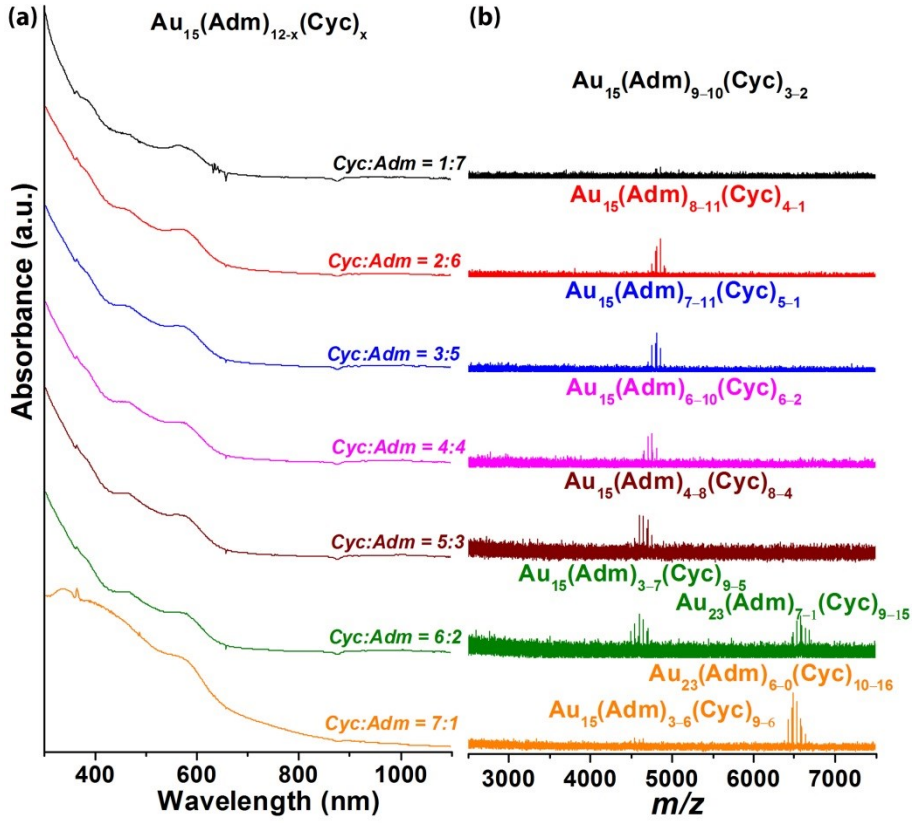

Figure S13. (a) UV−vis absorption and (b) ESI-MS spectra of heteroleptic $Au_{15}(Adm)_{12-x}(Cyc)_x$ NCs synthesized with the feeding ratios of Cyc : Adm = 1 : 7 (black curve), 2 : 6 (red curve), 3 : 5 (blue curve), 4 : 4 (pink curve), 5 : 3 (wine curve), 6 : 2 (green curve), and 7 : 1 (orange curve). At Cyc-to-Adm ratios of 6 : 2 and 7 : 1, besides $Au_{15}(Adm)_{12-x}(Cyc)_x$ NCs, some $Au_{23}(Adm)_{16-x}(Cyc)_x$ NCs can also be observed in the ESI-MS spectra.

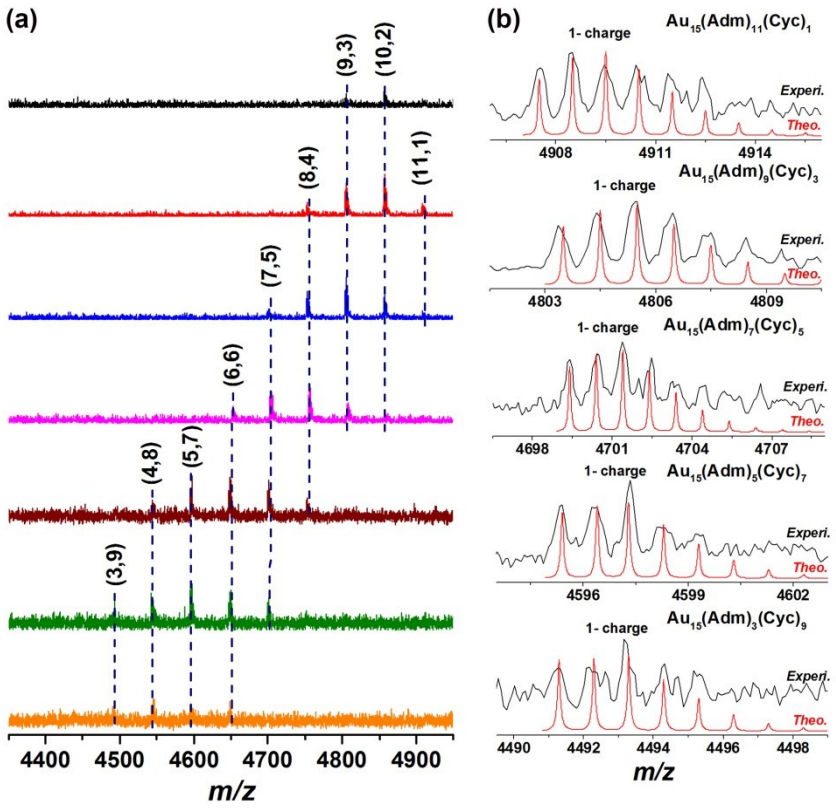

Figure S14. (a) Enlarged ESI-MS spectra of heteroleptic $Au_{15}(Adm)_{12-x}(Cyc)_x$ NCs synthesized with the feeding ratios of Cyc : Adm = 1 : 7 (black curve), 2 : 6 (red curve), 3 : 5 (blue curve), 4 : 4 (pink curve), 5 : 3 (wine curve), 6 : 2 (green curve), and 7 : 1 (orange curve). The numbers (11, 1), (10, 2), (9, 3), (8, 4), (7, 5), (6, 6), (5, 7), (4, 8), and (3, 9) labelled in the Figure represent $Au_{15}(Adm)_{11}(Cyc)_1$ NCs, $Au_{15}(Adm)_{10}(Cyc)_2$ NCs, $Au_{15}(Adm)_9(Cyc)_3$ NCs, $Au_{15}(Adm)_8(Cyc)_4$ NCs, $Au_{15}(Adm)_7(Cyc)_5$ NCs, $Au_{15}(Adm)_6(Cyc)_6$ NCs, $Au_{15}(Adm)_5(Cyc)_7$ NCs, $Au_{15}(Adm)_4(Cyc)_8$ NCs, and $Au_{15}(Adm)_3(Cyc)_9$ NCs, respectively. (b) Isotope patterns acquired theoretically (red curve) and experimentally (black curve) for $Au_{15}(Adm)_{11}(Cyc)_1$ NC species, $Au_{15}(Adm)_9(Cyc)_3$ NC species, $Au_{15}(Adm)_7(Cyc)_5$ NC species, $Au_{15}(Adm)_5(Cyc)_7$ NC species, and $Au_{15}(Adm)_3(Cyc)_9$ NC species.

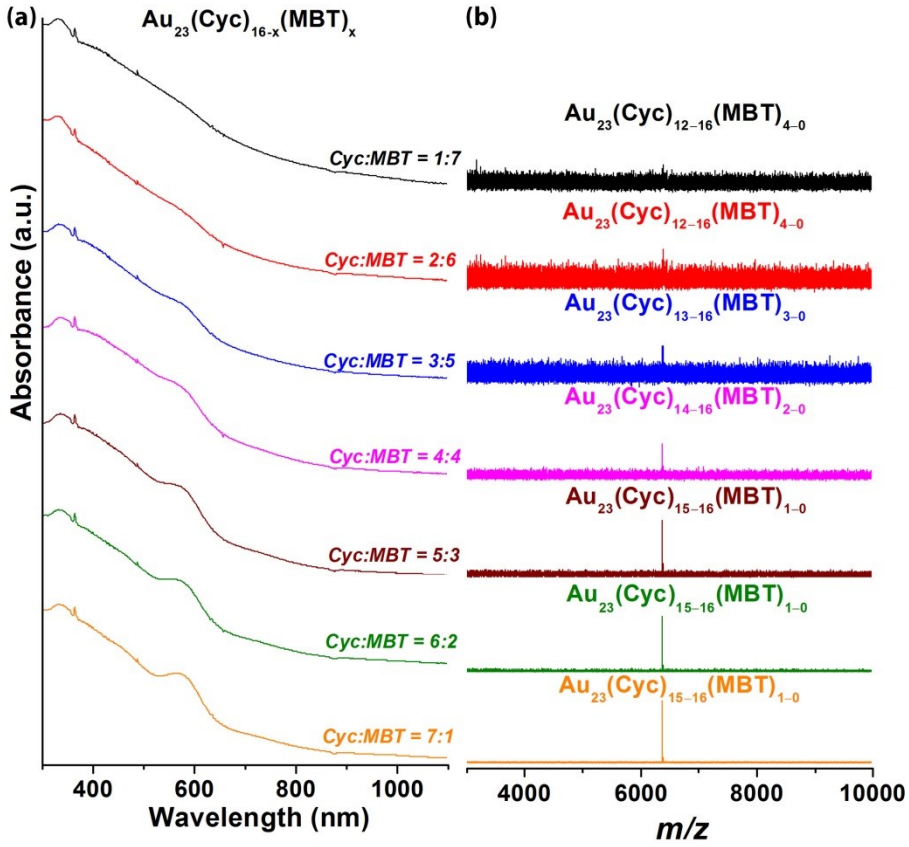

Figure S15. (a) UV−vis absorption and (b) ESI-MS spectra of heteroleptic $Au_{23}(Cyc)_{16-x}(MBT)_x$ NCs synthesized with the feeding ratios of Cyc : MBT = 1 : 7 (black curve), 2 : 6 (red curve), 3 : 5 (blue curve), 4 : 4 (pink curve), 5 : 3 (wine curve), 6 : 2 (green curve), and 7 : 1 (orange curve).

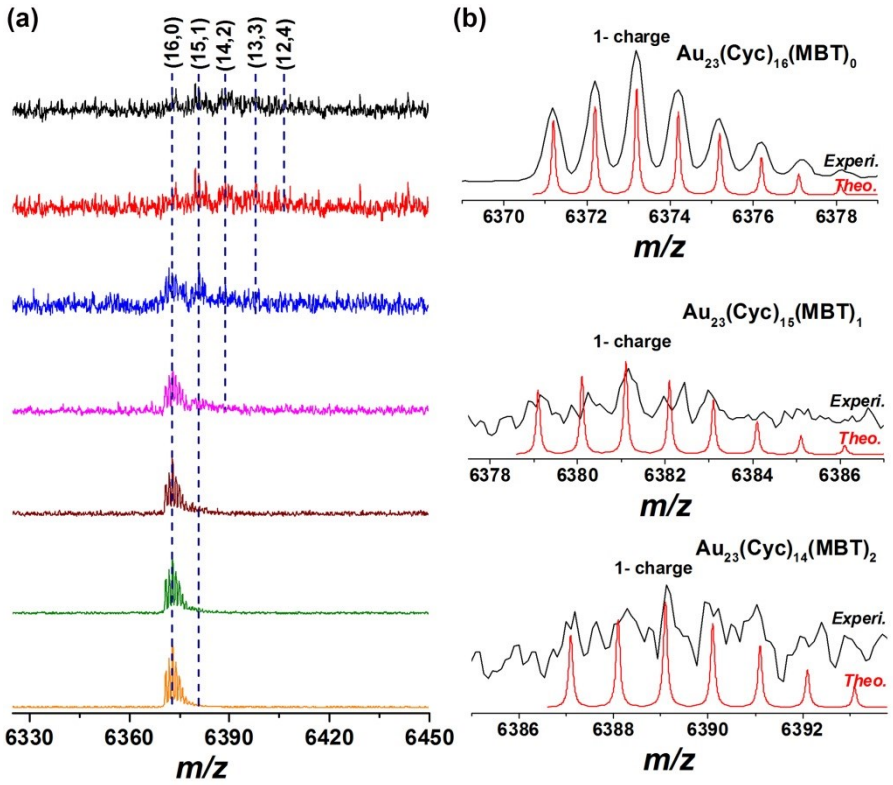

Figure S16. (a) Enlarged ESI-MS spectra of heteroleptic $Au_{23}(Cyc)_{16-x}(MBT)_x$ NCs synthesized with the feeding ratios of Cyc : MBT = 1 : 7 (black curve), 2 : 6 (red curve), 3 : 5 (blue curve), 4 : 4 (pink curve), 5 : 3 (wine curve), 6 : 2 (green curve), and 7 : 1 (orange curve). The numbers (16, 0), (15, 1), (14, 2), (13, 3), and (12, 4) labelled in the Figure represent $Au_{23}(Cyc)_{16}(MBT)_0$ NCs, $Au_{23}(Cyc)_{15}(MBT)_1$ NCs, $Au_{23}(Cyc)_{14}(MBT)_2$ NCs, $Au_{23}(Cyc)_{13}(MBT)_3$ NCs, and $Au_{23}(Cyc)_{12}(MBT)_4$ NCs, respectively. (b) Isotope patterns acquired theoretically (red curve) and experimentally (black curve) for $Au_{23}(Cyc)_{16}(MBT)_0$ NC species (top panel), $Au_{23}(Cyc)_{15}(MBT)_1$ NC species (middle panel), and $Au_{23}(Cyc)_{14}(MBT)_2$ NC species (bottom panel).

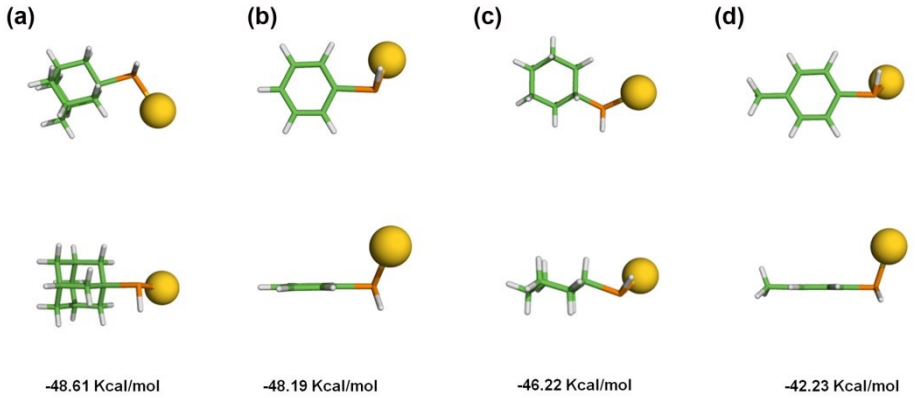

Figure S17. Computationally determined structures for 1 : 1 ligand-Au(I) complexes at the B3LYP/6-311G+(2d,p) level in toluene. All the CPK models were built based on the van der Waals radius. The yellow atom is Au(I). The corresponding binding energies between Au(I) and (a) an Adm ligand, (b) a PhSe ligand, (c) a Cyc ligand, and (d) a MBT ligand.

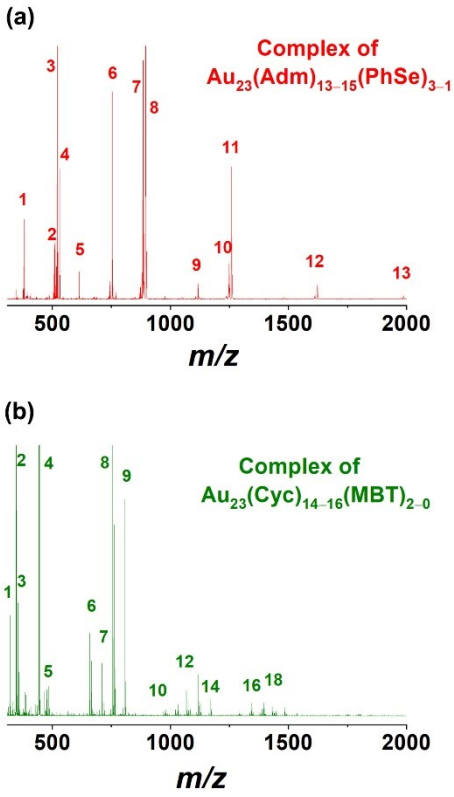

(c)

	Complex of	
	$Au_{23}(Adm)_{13-15}(PhSe)_{3-1}$	$Au_{23}(Cyc)_{14-16}(MBT)_{2-0}$
1	$AuCl_4(NaOH)$	Au(MBT)
2	$Au(PhSe)_2$	Au(Cyc)Cl
3	Au(Adm)(PhSe)	Au(MBT)Cl
4	$Au(Adm)_2$	$Au(MBT)_2$
5	$Au(Adm)_2(NaOH)_2$	$Au(Cyc)_2(NaOH)$ Au(Cyc)(MBT)(NaOH) $Au(MBT)_2(NaOH)$
6	$Au_2(PhSe)_2Cl$ $Au_2(Adm)(PhSe)Cl$	$Au_2(Cyc)_2Cl$ $Au_2(Cyc)(MBT)Cl$
7	$Au_2(Adm)_2(PhSe)$	$Au_2(MBT)_2Cl_2$ $Au_2(MBT)_2(NaOH)_2$
8	$Au_2(Adm)_3$	$Au_2(MBT)_2(Cyc)$ $Au_2(MBT)_3$
9	$Au_3(Adm)(PhSe)_2Cl$ $Au_3(Adm)_2(PhSe)Cl$	$Au_3(Cyc)_3Cl$ $Au_3(Cyc)_2(MBT)Cl$ $Au_3(Cyc)(MBT)_2Cl$ $Au_3(MBT)_3Cl$
10	$Au_3(Adm)_2(PhSe)_2$ $Au_3(Adm)_3(PhSe)$	$Au_3(Cyc)(MBT)_2Cl_2$ $Au_3(MBT)_3Cl_2$
11	$Au_3(Adm)_4$	$Au_3(Cyc)_2(MBT)_2$ $Au_3(Cyc)(MBT)_3$ $Au_3(MBT)_4$
12	$Au_4(Adm)_3(PhSe)_2$ $Au_4(Adm)_4(PhSe)$ $Au_4(Adm)_5$	$Au_4(Cyc)_2$ $Au_4(Cyc)(MBT)$
13	$Au_5(Adm)_5(PhSe)$ $Au_5(Adm)_6$	$Au_4(Cyc)(MBT)Cl$ $Au_4(MBT)_2Cl$
14		$Au_4(Cyc)_4Cl$ $Au_4(Cyc)_3(MBT)Cl$ $Au_4(Cyc)_2(MBT)_2Cl$
15		$Au_4(Cyc)_2(MBT)_2Cl_2$ $Au_4(Cyc)(MBT)_3Cl_2$ $Au_4(MBT)_4Cl_2$
16		$Au_4(Cyc)_3(MBT)_2$ $Au_4(Cyc)_2(MBT)_3$ $Au_4(Cyc)(MBT)_4$ $Au_4(MBT)_5$
17		$Au_4(Cyc)(MBT)_4Cl$ $Au_4(MBT)_5Cl$ $Au_5(Cyc)_4$
18		$Au_5(Cyc)_4Cl$ $Au_5(Cyc)_3(MBT)Cl$

Figure S18. ESI mass spectra (in negative mode) of complex precursors before the reduction for synthesizing heteroleptic Au NCs: complexes correspond to (a) $Au_{23}(Adm)_{5-6}(PhSe)_{11-10}$ NCs, and (b) $Au_{23}(Cyc)_{14-16}(MBT)_{2-0}$ NCs. (c) Molecular formulas of the labelled species.

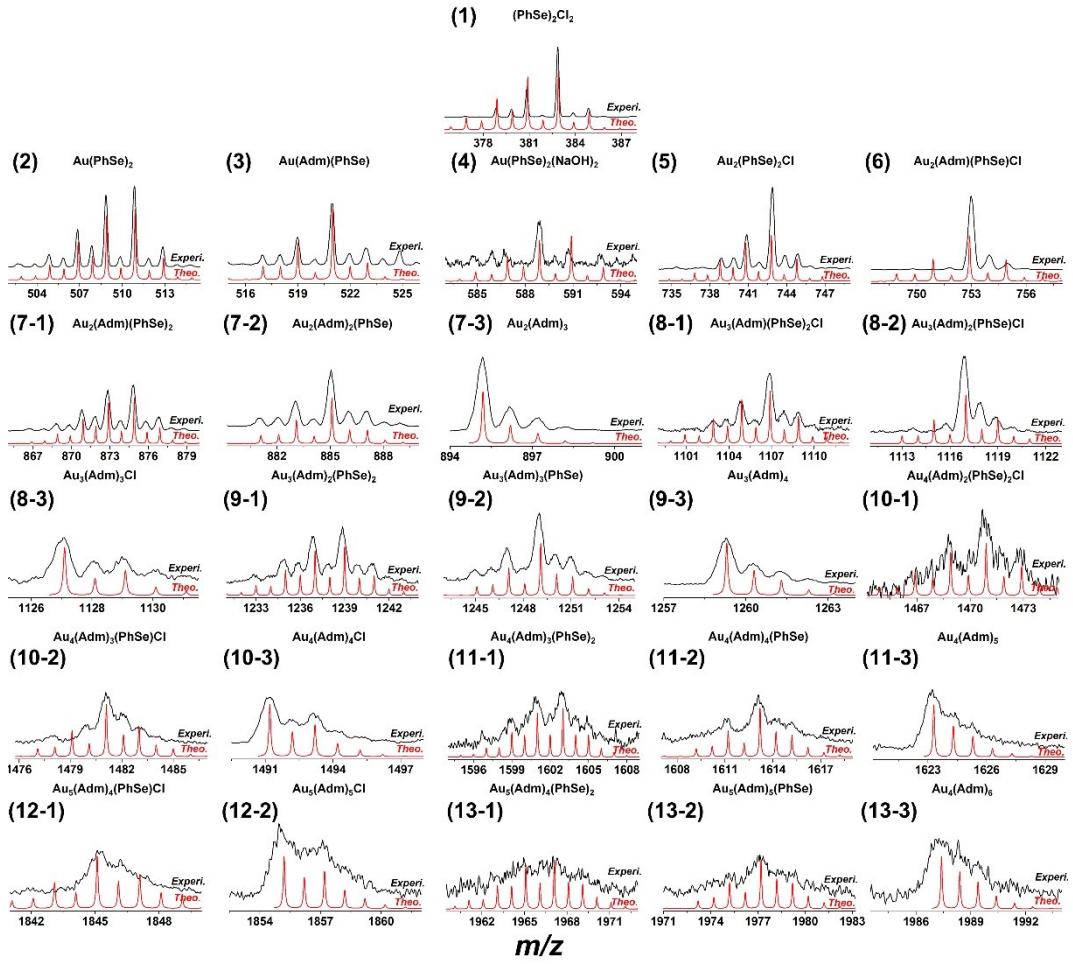

Figure S19. Isotope patterns acquired theoretically (red curve) and experimentally (black curve) for complex species #1–13 identified in the precursors of $Au_{41}(Adm)_8(PhSe)_{18}$ NCs.

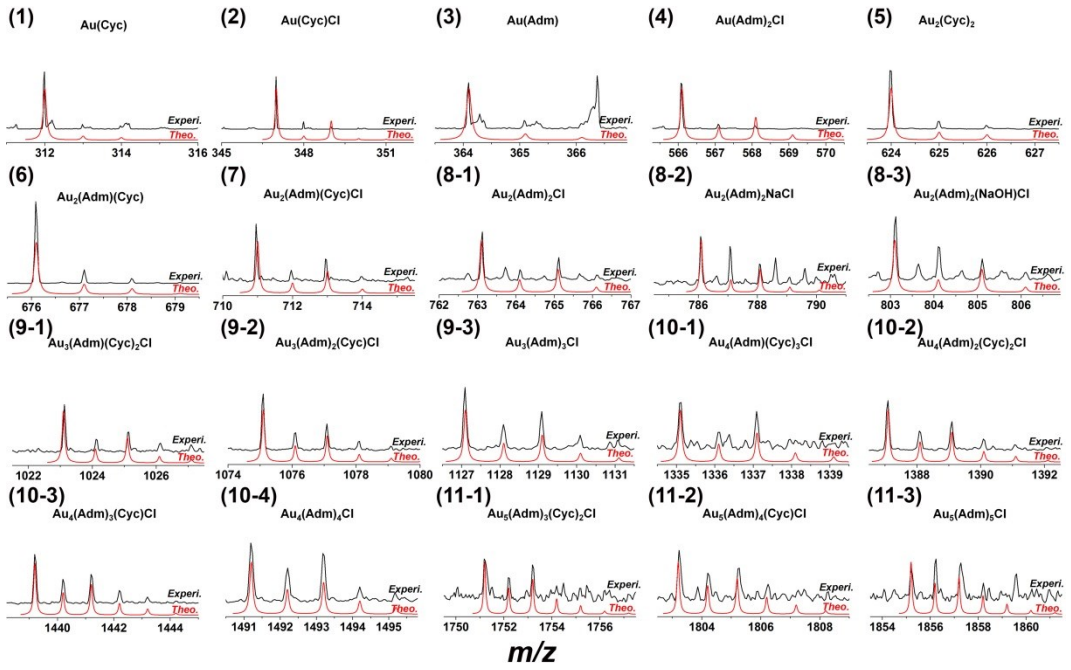

Figure S20. Isotope patterns acquired theoretically (red curve) and experimentally (black curve) for complex species #1–11 identified in the precursors of $Au_{15}(Adm)_{6–10}(Cyc)_{6–2}$ NCs.

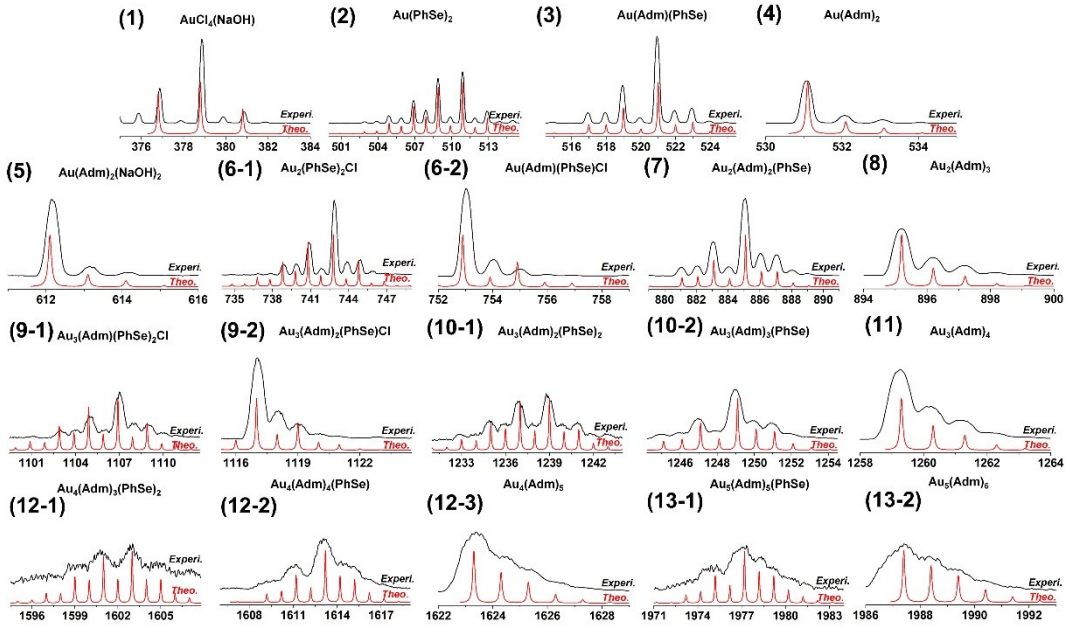

Figure S21. Isotope patterns acquired theoretically (red curve) and experimentally (black curve) for complex species #1-13 identified in the precursors of $Au_{23}(Adm)_{13–15}(PhSe)_{3–1}$ NCs.

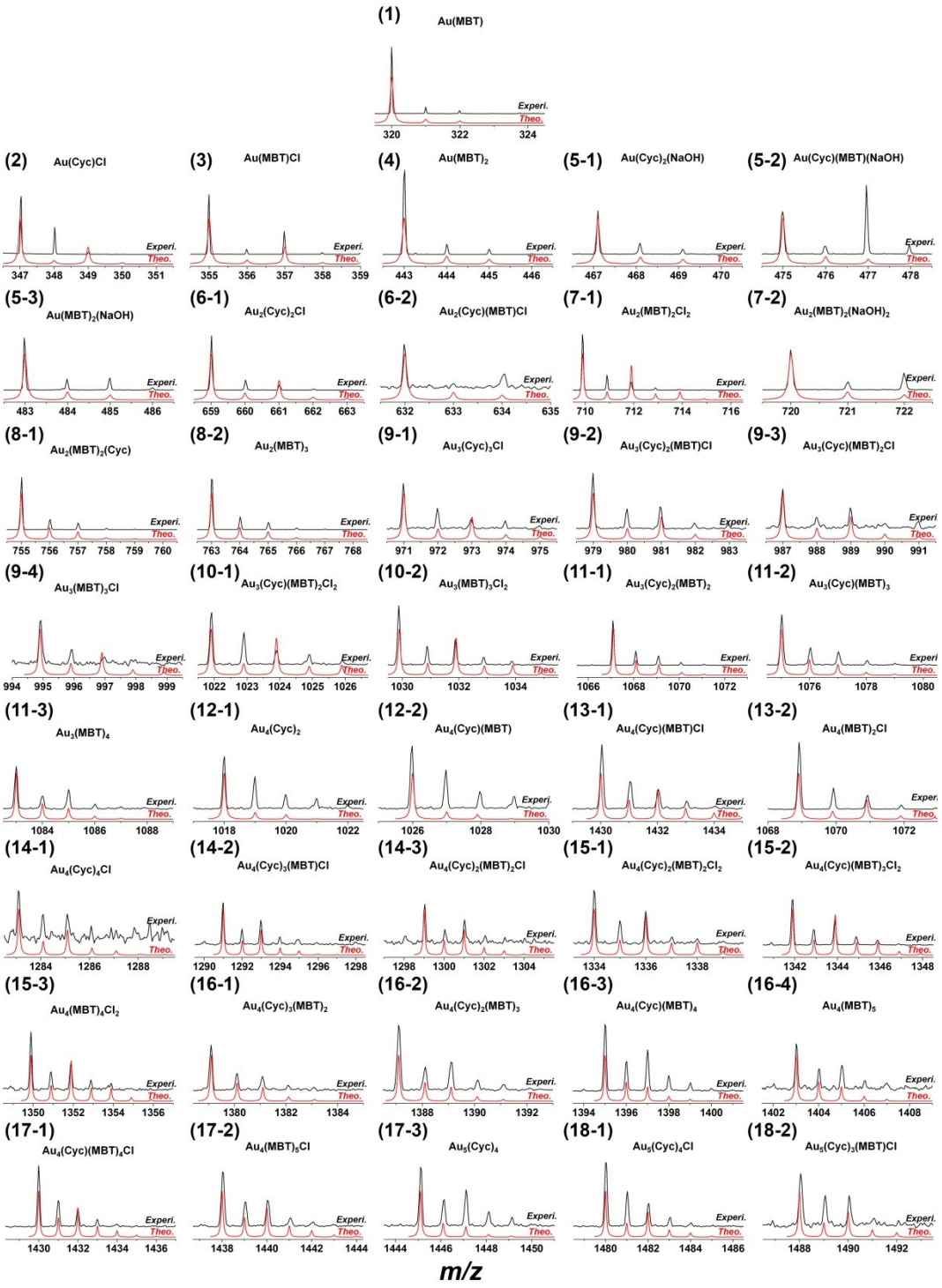

Figure S22. Isotope patterns acquired theoretically (red curve) and experimentally (black curve) for complex species #1–18 identified in the precursors of $Au_{23}(Cyc)_{14–16}(MBT)_{2–0}$ NCs.

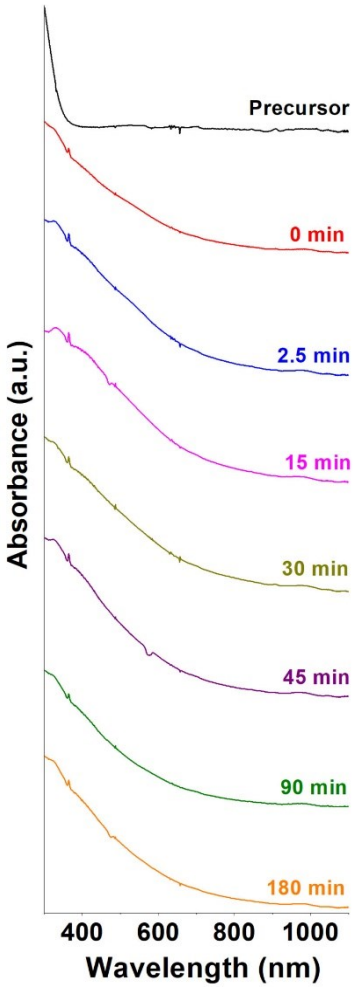

Figure S23. Time evolution of UV-vis absorption spectra of the reaction solution during the synthesis of $Au_{41}(Adm)_8(PhSe)_{18}$ NCs.

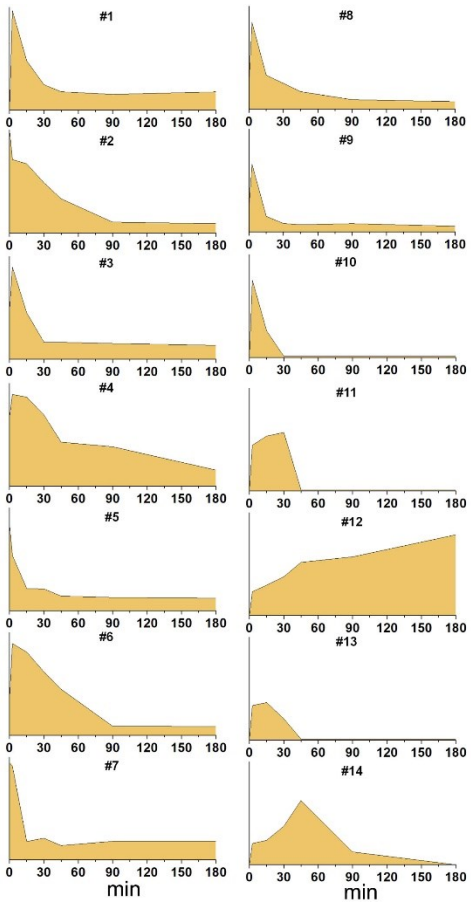

Figure S24. Time-dependent abundance of the main complexes and NC species during the formation process of $Au_{41}(Adm)_8(PhSe)_{18}$ NCs. Species #1: $Au_1(PhSe)_1$, $Au_1(Adm)_1$, $Au_1(PhSe)_1Cl$; Species #2: $Au_1(PhSe)_2$, $Au_1(Adm)_2$; Species #3: $Au_2(Adm)_{1\text{-}2}(PhSe)_{1\text{-}0}$, $Au_2(Adm)_{1\text{-}0}(PhSe)_{1\text{-}2}Cl$; Species #4: $Au_2(Adm)_{1\text{-}3}(PhSe)_{2\text{-}0}$; Species #5: $Au_3(Adm)_{2\text{-}3}(PhSe)_{1\text{-}0}$, $Au_3(Adm)_{1\text{-}2}(PhSe)_{2\text{-}1}Cl$; Species #6: $Au_3(Adm)_{2\text{-}4}(PhSe)_{2\text{-}0}$; Species #7: $Au_4(Adm)_4$, $Au_4(Adm)_{2\text{-}4}(PhSe)_{2\text{-}0}Cl$; Species #8: $Au_4(Adm)_{3\text{-}5}(PhSe)_{2\text{-}0}$; Species #9: $Au_5(Adm)_{4\text{-}6}(PhSe)_{2\text{-}0}$; Species #10: $Au_{14}(Adm)_1(PhSe)_{12}$; Species #11: $Au_{15}(Adm)_{11\text{-}12}(PhSe)_{1\text{-}0}$, $Au_{15}(Adm)_1(PhSe)_{12}$; Species #12: $Au_{41}(Adm)_8(PhSe)_{18}$; Species #13: $Au_{21}(Adm)_{13\text{-}14}(PhSe)_{1\text{-}0}$; Species #14: $Au_{23}(Adm)_{14}(PhSe)_2$.

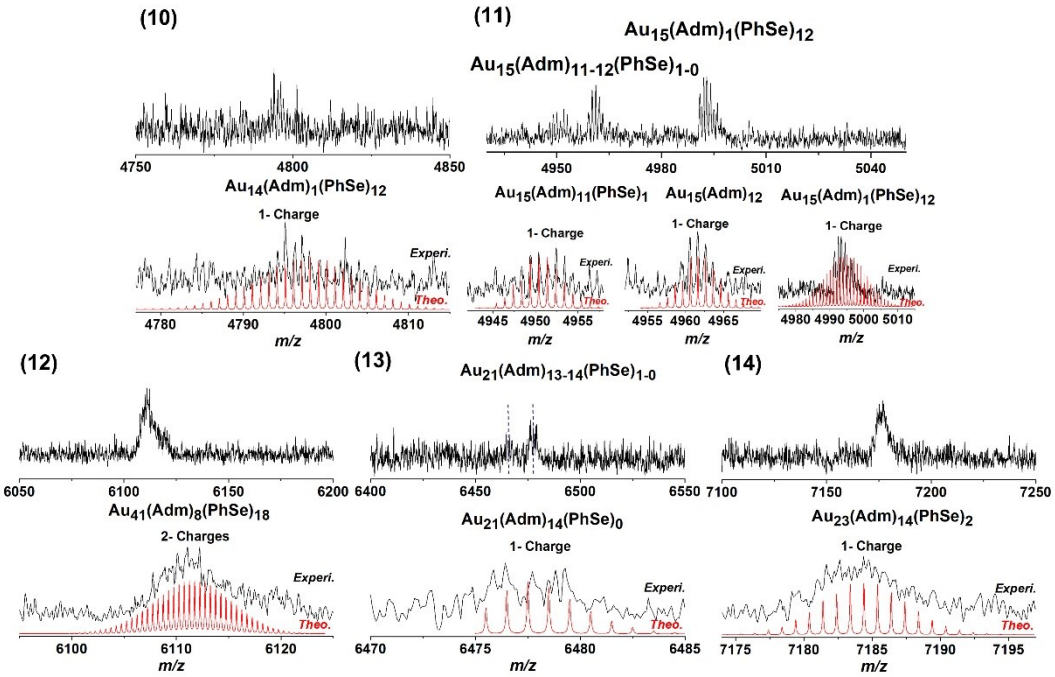

Figure S25. Enlarged ESI-MS spectra (upper panels) and isotope patterns (lower panels) acquired theoretically (red curve) and experimentally (black curve) for intermediate NC species #10–14 identified during the synthesis of $Au_{41}(Adm)_8(PhSe)_{18}$ NCs.

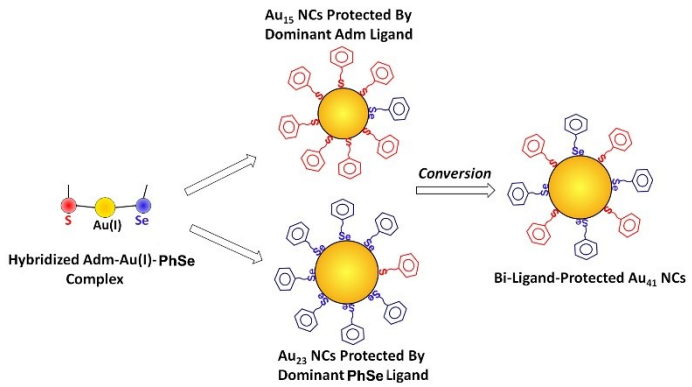

Figure S26. The proposed synthetic mechanism for the heteroleptic $Au_{41}(Adm)_8(PhSe)_{18}$ NCs.

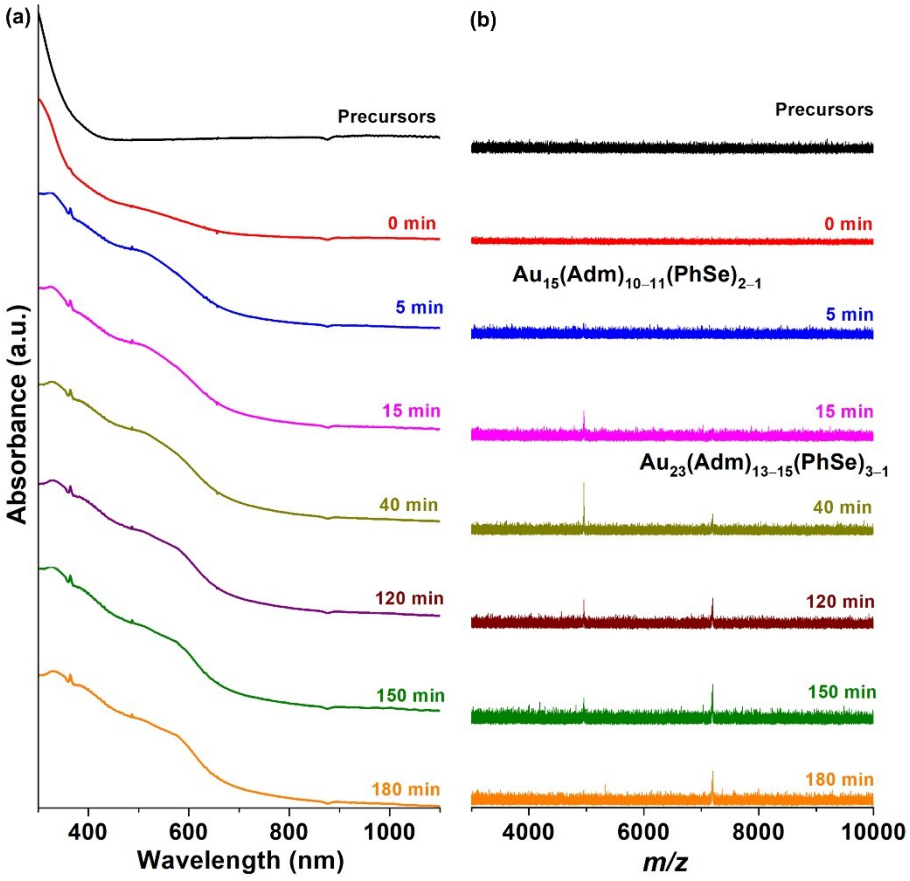

Figure S27. Time evolution of (a) UV–vis absorption and (b) ESI-MS spectra of the reaction solution during the synthesis of $Au_{23}(Adm)_{13–15}(PhSe)_{3–1}$ NCs.

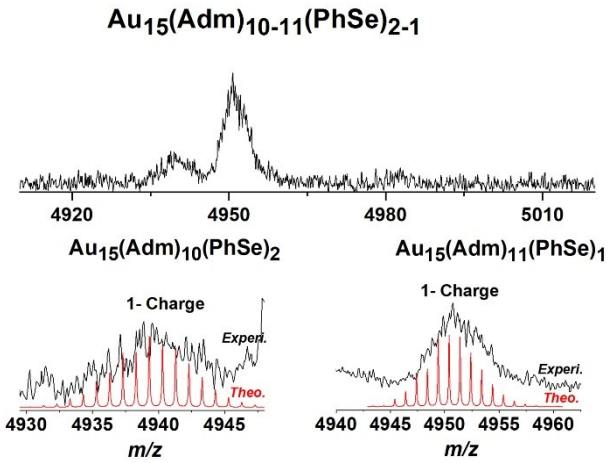

Figure S28. Enlarged ESI-MS spectrum (upper panel) and isotope patterns acquired theoretically (red curve) and experimentally (black curve) for intermediate NC species identified during the synthesis of $Au_{23}(Adm)_{13–15}(PhSe)_{3–1}$ NCs displayed in Figure S27.

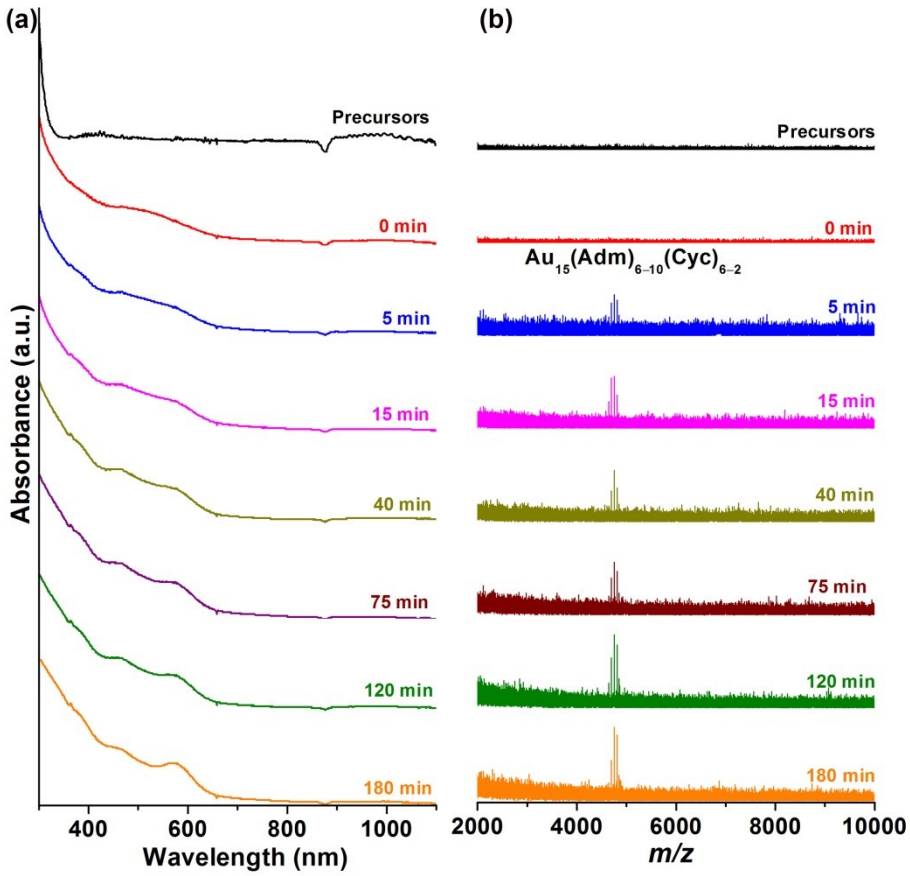

Figure S29. Time evolution of (a) UV–vis absorption and (b) ESI-MS spectra of the reaction solution during the synthesis of $Au_{15}(Adm)_{6–10}(Cyc)_{6–2}$ NCs.

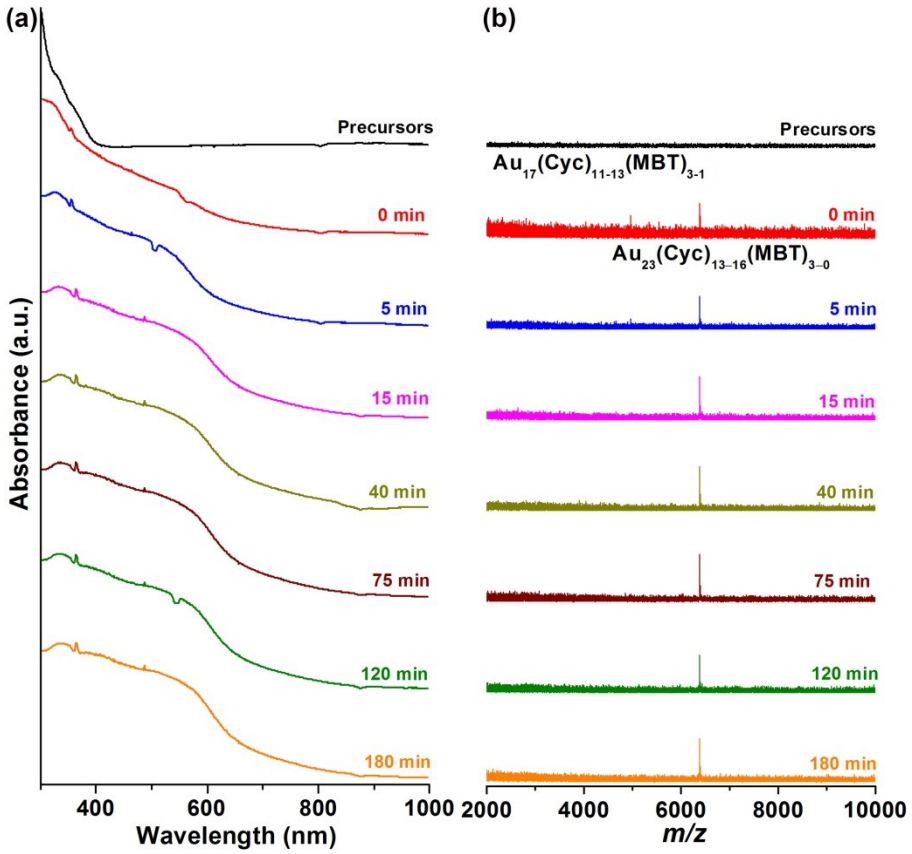

Figure S30. Time evolution of (a) UV–vis absorption and (b) ESI-MS spectra of the reaction solution during the synthesis of $Au_{23}(Cyc)_{13–16}(MBT)_{3–0}$ NCs.

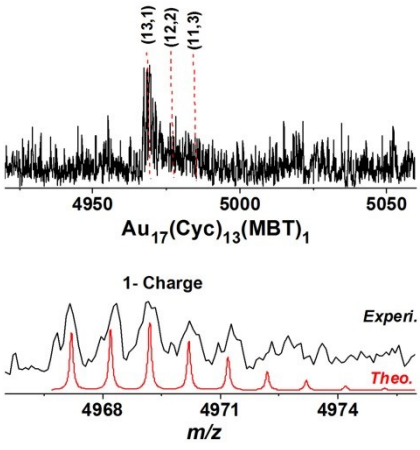

Figure S31. Enlarged ESI-MS spectrum (upper panel) and isotope patterns (lower panel) acquired theoretically (red curve) and experimentally (black curve) for intermediate NC species identified during the growth process of $Au_{23}(Cyc)_{13–16}(MBT)_{3–0}$ NCs displayed in Figure S30. The numbers (13, 1), (12, 2), and (11, 3) labelled in the Figure represent $Au_{17}(Cyc)_{13}(MBT)_1$ NCs, $Au_{17}(Cyc)_{12}(MBT)_2$ NCs, and $Au_{17}(Cyc)_{11}(MBT)_3$ NCs, respectively.